

Magnetocaloric effect enhancement driven by intrinsic defects in Ni-Mn-Sn-Co alloys

V. Sánchez-Alarcos^{1,2*}, J. López-García^{1,3}, I. Unzueta^{4,5}, J. I. Pérez-Landazábal^{1,2}, V. Recarte^{1,2}, J.J. Beato-López^{1,2}, J.A. García^{5,6}, F. Plazaola⁴ and J. A. Rodríguez-Velamazán³

¹ Departamento Física. Universidad Pública de Navarra, Campus de Arrosadia, 31006 Pamplona, Spain

² Institute for Advanced Materials (INAMAT), Universidad Pública de Navarra, Campus de Arrosadia, 31006 Pamplona, Spain

³ Institut Laue Langevin, 71, Avenue des Martyrs, 38042 Grenoble Cedex, France

⁴ Elektrizitate eta Elektronika Saila, Euskal Herriko Unibersitatea UPV/EHU, p.k. 644, 48080 Bilbao, Spain

⁵ BC Materials (Basque Centre for Materials, Applications and Nanostructures), 48080 Leioa, Spain

⁶ Fisika Aplikatua II Saila, Euskal Herriko Unibersitatea UPV/EHU, p.k. 644, 48080 Bilbao, Spain

*Corresponding author: *Tel.*: +34 948 169582; *Fax.*: +34 948 169565

E-mail address: vicente.sanchez@unavarra.es

Abstract.

The influence of mechanically-induced defects on the magnetostructural properties is analyzed in a Ni-Co-Mn-Sn alloy subjected to soft milling and subsequent annealing treatments. It is found that, opposite to what occurs in Ni-Mn-Sn ternary alloys, the annealing treatment affects the magnetic properties in a different way in martensite and in austenite. In particular, the saturation magnetization significantly increases in martensite after annealing whereas just a very slight variation is observed in austenite. This leads to the interesting fact that the presence of microstructural defects, far from worsening, makes the magnetocaloric effect to be higher in the as-milled state than after annealing. This behavior is explained as the result of the combination of the effect of defects on the Mn-Mn distance, the effect Co on the magnetic exchange coupling between Mn atoms, and the effect of defects on the vibrational entropy change at the martensitic transformation.

Keywords: Ni-Mn-Sn-Co, magnetocaloric effect, defects, vibrational entropy

1. INTRODUCTION

Ni-Mn-based metamagnetic shape memory alloys are being widely studied during the last decade because of the unique multifunctional features they show as a result of the interplay between a structural transformation and a complex magnetic ordering. Due to the strong dependence of the magnetic exchange interactions on the Mn-Mn distances [1-3], the change in the interatomic distances caused by the occurrence of a thermoelastic martensitic transformation (MT) in some of these alloys results in a large magnetization change (ΔM) at the transformation temperature that favors the induction of the structural transformation by an applied magnetic field [4-7]. Such magnetic induction of the MT, and the different features of the different structural phases (austenite and martensite), give rise to interesting properties such as the magnetic shape memory effect, large magnetoresistance or giant inverse magnetocaloric effect, that make these alloys very attractive for practical applications in sensing and magnetic refrigeration [8-14].

The most promising alloys for magnetocaloric applications are those alloys in the Ni-Mn-X (X=In, Sn, and Sb) systems in which the MT takes place between a ferromagnetic austenite and a weaker-magnetic martensite. The MT characteristics and the magnetic properties of these alloys depend on composition, atomic order and, to a lesser extent, on microstructure. The compositional dependence has been widely studied, being the complete phase diagrams of the appearing structural and magnetic phases well established [15-18]. Atomic order has been also systematically studied. In Ni-Mn-In and Ni-Mn-In-Co alloys it has been shown that the magnetostructural properties can be properly tuned varying the long-range atomic order, which can be easily controlled by means of thermal treatments [19-21]. In Ni-Mn-Sn and Ni-Mn-Sb alloys, in turn, the L2₁ structure is highly stable and the atomic order is then hardly modifiable by means of conventional thermal treatments [22]. In these alloys, the modification of the microstructural parameters (grain size, defects, internal stresses...) appears as almost the only way to modify the functional properties for a selected alloy composition. Mechanical milling and subsequent annealing treatments are one of the simplest and most used method to modify the microstructure. Typically, the grain size reduction and the presence of defects and internal stresses induced by

milling degrade the MT and the magnetic properties, which can be then partially restored upon microstructural recovery processes brought by subsequent annealing [23-28]. In this respect, by comparing a Ni-Mn-Sn alloy in both the as-milled and the annealed states, we have recently shown that, even though no appreciable long-range atomic disorder was induced by milling, the saturation magnetization of both martensitic and austenitic phases are considerably higher after annealing, due to the reduction of the density of the anti-phase boundaries (linked to dislocations) which promote the antiferromagnetic coupling between Mn moments [28]. A similar magnetic deterioration at anti-phase boundaries was indeed evaluated in Ni-Mn-Al-Ga alloys by electron holography, and explained as a consequence of a local atomic disordering in the boundary region [29].

The addition of Cobalt has been shown to enhance the magnetism of the austenite and to hinder ferromagnetic ordering in martensite in Ni-Mn-X alloys, thus leading to an increase of ΔM and therefore to larger magnetically-induced shifts of the MT temperature and higher associated magnetocaloric effects [4, 30-33]. In particular, in Ni-Mn-Sn alloys it has been also shown that the magnetic coupling between the Mn moments on the 4a (Mn sublattice) and 4b sites (Sn sublattice) of the austenitic cubic structure changes from being antiferromagnetic to ferromagnetic because of the substitution of Ni by Co [33] (while the magnetic coupling between Mn atoms on the 4a sites is ferromagnetic both in the ternary and the quaternary alloys). In this regard, it could be thought that the influence of the presence of anti-phase boundaries (and any other microstructural defect resulting in local atomic disordering) on the magnetic properties will be different in the quaternary Co-doped alloys to that in the ternary ones. In this sense, the effect of mechanically-induced defects on the magnetostructural properties, and in particular on the magnetocaloric effect, is analyzed on a quaternary Ni-Co-Mn-Sn alloy subjected to soft milling and subsequent annealing. It is found that the presence of microstructural defects, far from worsening, can make the magnetocaloric effect to be higher in the as-milled state than after subsequent annealing. This unusual beneficial presence of defects is explained as the result of the combination of the effect of defects on the Mn-Mn distance, the effect Co on the magnetic

exchange coupling between Mn atoms, and the effect of defects on the vibrational entropy change at the martensitic transformation.

2. EXPERIMENTAL

A $\text{Ni}_{45}\text{Co}_5\text{Mn}_{35}\text{Sn}_{15}$ alloy was prepared from high purity elements by arc melting under protective Ar atmosphere. The as-cast ingot was homogenized at 1173 K during 24h and then slowly cooled to RT. The composition was analyzed by EDS in a Jeol JSM-5610LV Scanning Electron Microscope (SEM). In order to induce defects, the alloy was subjected to hand milling in an agate mortar until reaching a uniform particle-size distribution. The mean particle size of the powder, estimated from SEM images, was $60 \pm 20 \mu\text{m}$. A part of the obtained powder was then annealed at 673 K for 5 minutes in order to remove some of the defects induced by milling. The microstructural states obtained in the as-milled and the annealed samples were then analyzed and compared: the martensitic transformations were characterized by differential scanning calorimetry (Q-100 DSC, TA Instruments), the magnetic properties by SQUID magnetometry (QD MPMS XL-7), and the crystallographic and magnetic structures were determined from powder neutron diffraction measurements performed on the D1B diffractometer, at the Institute Laue-Langevin (Grenoble, France), using a neutron wavelength of 1.28 Å. The structures were refined by the Rietveld method using the FullProf package programs [34].

3. RESULTS AND DISCUSSION

Figure 1a shows the temperature dependence of the magnetization in the as-milled and annealed samples under 100 Oe and 60 kOe applied magnetic fields. The sequences of magnetostructural transformations can be clearly determined from the low-field $M(T)$ curves: in both samples, the high temperature paramagnetic austenite becomes ferromagnetic around 360 K and a subsequent magnetization jump takes place around 180 K linked to the martensitic transformation to a weaker-magnetic martensite. The occurrence of such martensitic transformation is confirmed

from the appearance of exothermic and endothermic peaks, associated to the forward and reverse MT, respectively, in calorimetric measurements (see inset). The transformation temperatures and the magnetization change at the MT obtained from the different $M(T)$ curves are summarized in Table 1 along with the entropy change at MT, ΔS , estimated from the DSC thermograms. As it occurred in ternary Ni-Mn-Sn alloys [28], neither the Curie temperature, T_C^a , nor the MT temperature, T_M , seem to evolve substantially with the annealing treatment. Taking into account the high sensibility of these transition temperatures to long-range atomic order [35], the absence of evolution suggests a scarce effect of annealing on atomic order, as it could be indeed expected given the high stability of the $L2_1$ structure in the Ni-Mn-Sn system [22]. Likewise, the thermal hysteresis linked to the MT is also practically unaffected by annealing (in fact, it is slightly larger in the annealed sample). As shown in Figure 1b, the MT shifts toward lower temperatures under the application of a 60 kOe magnetic field, being the shift (with respect to T_M obtained at 100 Oe) almost the same in both the as-milled and the annealed samples. On the contrary, the magnetization change at the MT, ΔM , is definitively affected by annealing, being ΔM quite lower in the annealed sample.

The effect of annealing on the saturation magnetization, M_s , of the two structural phases is illustrated in Figure 2, where the magnetic-field dependence of magnetization is shown for both phases in both the as-milled and the annealed states. In all cases, the magnetization shows an initial abrupt increase and a subsequent trend to saturation, typical of ferromagnetic behavior. Interestingly, the annealing treatment affects the net value in a different way in martensite and in austenite. In particular, the saturation magnetization significantly increases in martensite after annealing ($\Delta M_s^{mart} / M_s^{mart} \sim 28\%$) whereas a very slight variation ($\Delta M_s^{aust} / M_s^{aust} \sim 3\%$) is observed in austenite. This behavior is quite surprising as long as it is opposite to what is found in similarly-milled ternary Ni-Mn-Sn alloys, for which the high-field magnetization increase linked to annealing is similar (even larger) in austenite to that in martensite [31].

In order to ascertain the origin of the different evolution of the saturation magnetization in martensite and austenite upon annealing, neutron diffraction measurements have been performed

in both phases of the as-milled and annealed samples. Figure 3 shows the obtained diffractograms together with the Rietveld refinement of the diffraction patterns. The nuclear structures have been first refined from diffractograms obtained at 400 K in paramagnetic austenite, which allowed a more accurate determination of the site occupancy, and then a combined nuclear and magnetic refinement has been performed for ferromagnetic austenite at 300 K and ferromagnetic martensite at 10K. The structural and magnetic parameters obtained after Rietveld refinement are shown in Table 2. Both in martensite and in austenite, the crystallographic structure is the same before and after annealing. The austenitic phases show the typical cubic $L2_1$ structure (space group $Fm\bar{3}m$) with almost the same lattice parameter. As expected, no significant variation of the atomic order is observed, in agreement with the null evolution of the structural and magnetic transition temperatures. Likewise, the martensitic structure is the same in both samples; a $3M$ modulated monoclinic structure (space group $P2_1/m$) with similar lattice parameters. With respect to the magnetic structure, it is first worth noting that the magnetic moments of Mn atoms are all positive in austenite, thus confirming the ferromagnetic coupling between Mn atoms, even between those in the 4a and 4b sites. On the contrary, negatives moments are obtained in martensite for Mn atoms in those sites resulting from the monoclinic distortion of the 4b sites (as expected due to the weakening of the exchange interactions as a consequence of the abrupt change in the Mn–Mn interatomic distances upon the MT [36]). Interestingly, the net magnetic moments in austenite are unaffected by annealing whereas a significant influence of annealing is observed on the magnetic moments in martensite, in which a marked decrease in the negative antiferromagnetic contribution is observed.

Since neither crystallographic structure nor lattice parameters nor long-range atomic order evolve upon annealing, the observed evolution of the saturation magnetization and the magnetic moments in martensite must be purely attributable to a microstructural relaxation, just as it occurs in a similarly-milled ternary Ni-Mn-Sn alloy [31]. In that case, the increase of the saturation magnetization of austenite and martensite after annealing was ascribed to a reduction of the density of anti-phase boundaries as a result of the annihilation of superlattice dislocations. In the

cubic phase of the ternary Ni-Mn-Sn alloys, the magnetic coupling between Mn atoms in the 4a sites is ferromagnetic whereas it is antiferromagnetic between Mn atoms in the 4a and 4b sites [21]. Hence, the magnetic coupling between Mn atoms may change from ferromagnetic to antiferromagnetic across linear or planar defects, thus leading to a decrease in the net magnetic moment. In the austenitic phase of the quaternary alloy, in turn, the presence of Co on the Ni sites makes the Mn atoms at the 4a and 4b sites to couple ferromagnetically, and therefore the magnetic coupling between Mn atoms (whether nearest or next-nearest neighbors) will be always ferromagnetic, irrespectively of the presence of defects. Therefore, assuming that a similar annihilation process occurs on annealing the quaternary alloy, the almost null evolution of the saturation magnetization of austenite can be explained as a direct consequence of the ferromagnetic coupling between Mn atoms. With respect to the martensitic phase, the weakening of the magnetic exchange interactions upon the martensitic transformation makes the Mn atoms in the martensitic structure to couple antiferromagnetically or ferrromagnetically depending on whether they are nearest or next-nearest neighbors, respectively, both in the ternary and the quaternary alloys. Therefore, the change of the Mn-Mn distance associated to the presence of defects (or even to internal stresses) may explain the lower antiferromagnetic contribution in the annealed sample, where the amount of defects is presumably lower than in the as-milled one.

The effect of defects on the magnetic properties can be qualitatively estimated from the fitting of the field-dependence of the magnetization to the classical law of approach to saturation for magnetization

$$M = M_s \left(1 - \frac{a}{H} - \frac{b}{H^2} \right) + \chi H \quad (1)$$

where H is the applied field, M_s the saturation magnetization, χ the field independent susceptibility and a and b are coefficients related to magnetic and structural properties of the sample [36-39]. In particular, the parameter a depends on the stresses field created by dislocations and non-magnetic inclusions and it can be approximated to $a \approx 4\pi\rho M_s P_{eff}$, where ρ is the density of the material and P_{eff} is the effective fraction of porosity and non-magnetic inclusions [40]. From the

fitting of the magnetization curves in martensite to the law of approach to saturation, shown in Figure 4, P_{eff} values of 0.021 and 0.014 are obtained for the as-milled and annealed samples, respectively. The higher value of effective fraction of non-magnetic inclusions in the as milled sample points out that the density of dislocations where the ferromagnetic coupling is lost by the local atomic disordering is higher in the as-milled sample than in the annealed one, in agreement with the expected reduction of defects upon heating treatment.

Since the magnetically-induced shift of T_M is directly related to ΔM through the Clausius-Clapeyron equation

$$\frac{dT_M}{dH} = -\mu_0 \frac{\Delta M}{\Delta S} \quad (2)$$

(where H is the applied magnetic field), the observed effect of annealing on the magnetic moments, and in particular on ΔM , suggests a possible influence of the mechanically-induced defects on the magnetic induction of the MT and therefore on the magnetocaloric effect (MCE). The effect of magnetic field on the MT temperature has been analyzed from the temperature dependence of magnetization under different applied magnetic fields. Figure 5a shows the $M(T)$ curves obtained on heating under applied magnetic fields ranging from 100 Oe to 60 kOe around the martensitic transformation of the as-milled and the annealed samples. As expected, in both cases the magnetization jump associated to the MT occurs at lower temperatures on increasing the magnetic field, because of the magnetic stabilization of the austenite. The shift of T_M (determined from the peaks of the derivative curve of magnetization measurements) is shown in Figure 5b as a function of the applied field. The transformation temperatures linearly decrease with the increasing applied field, being the slope the same in both samples, $dT_M/dH \approx 0.5$ K/kOe. It is worth noting that this slope is in agreement with the dT_M/dH values calculated by substituting into Equation 1 the values of ΔM and ΔS shown in Table 1.

The MCE, which can be defined as the entropy change in isothermal conditions, ΔS_{iso} , has been calculated from the ZFC magnetization measurements shown in Figure 5a by numerical integration of the derivative of the magnetization with respect to temperature, according to the expression

$$\Delta S_{iso} = S(T, H) - S(T, 0) = \int_0^H \left(\frac{\partial M}{\partial T} \right)_H dH \quad (3)$$

The obtained ΔS_{iso} values are shown in Figure 6 as a function of both temperature and applied magnetic field. In both cases, a positive peak (inverse MCE) is observed linked to the magnetostructural transformation at T_M^{rev} . The MCE values increase with the increasing magnetic field, being the highest calculated values of the magnetically-induced entropy change those obtained for the highest applied field. In order to better compare the magnitude of the MCE, the ΔS_{iso} values obtained under 60 kOe in both samples are plotted together as a function of temperature in Figure 7. It can be seen that the magnetocaloric effect is considerably higher in the as-milled sample ($\Delta S_{iso}^{A-M} \approx 8$ J/kgK and $\Delta S_{iso}^{Ann} \approx 6$ J/kgK) in spite of containing presumably a higher amount of defects. Interestingly, this result suggest that the presence of defects, far from worsening, may be beneficial for MCE in metamagnetic Heusler alloys.

Since the magnetically-induced entropy change (that is, the MCE) in this alloy comes from the magnetic induction of the MT (due to different exchange interactions in martensite and austenite), the fact that both the magnetically-induced shift of the MT temperature and the width of the MT temperature range is almost the same in both samples implies that a similar fraction of the MT is induced by the application of the magnetic field in both samples. Therefore, the higher ΔS_{iso} obtained in the as-milled sample must be due to its higher total entropy change at the MT with respect to that in the annealed sample (see table 1). The entropy change linked to the MT (which is the limit value of the attainable ΔS_{iso}) can be considered as the sum of a vibrational, ΔS_{vib} , and a magnetic, ΔS_{mag} , term, in such a way that $\Delta S \approx \Delta S_{vib} + \Delta S_{mag}$ (the small electronic term is usually neglected) [42]. For the martensite to austenite transformation in metamagnetic shape memory alloys (in which $\Delta M > 0$), the vibrational and the magnetic terms are positive and negative, respectively, the vibrational one being necessarily higher [42]. Since ΔS_{mag} is directly related to ΔM , and it is higher in the as-milled sample, a higher magnetic contribution opposing the vibrational one should be expected in the as-milled sample, which would lead to a lower net ΔS . In this sense, the circumstance that ΔS is actually higher in the as-milled sample implies that ΔS_{vib} must be considerably higher in the as-milled sample than in the treated one. Taking into account

that the crystallographic structures are exactly the same in both samples, the deduced difference in ΔS_{vib} (and therefore in ΔS) can be then attributable to the decrease in the concentration of mechanically-induced defects upon annealing (in spite of ΔS typically increases because of the microstructural recovery brought by annealing, as in fact occurs in ternary Ni-Mn-Sn alloys [43]). Although the influence of defects (point defects, dislocations and anti-phase boundaries) in the vibrational properties of some metals has been analyzed in several theoretical studies [44-46], up to our knowledge this is the first indirect evidence of the effect of defects on the vibrational entropy change at the martensitic transformation. In any case, further works on the analysis of the type and concentration of defects should be needed in order to quantitatively correlate defects and magnetically-induced entropy change.

3. SUMMARY AND CONCLUSIONS

The influence of mechanically-induced defects on the magnetostructural properties is analyzed in a Ni-Co-Mn-Sn alloy. It is found that the mechanically-induced defects, far from worsening, improve the magnetocaloric response. This is due to two main features; first, the different exchange coupling between nearest-neighbors Mn atoms in the austenitic and in the martensitic structures makes the magnetization change at the martensitic transformation to be increased as a result of the presence of defects. Second, the mechanically-induced defects increase the vibrational entropy change at the transformation, thus leading to a higher total entropy change and, therefore, to a higher attainable magnetocaloric effect. Given the difficulty to modify the atomic order in the Ni-Mn-Sn system by means of conventional thermal treatments, the presented results show that, once fixed the composition, the induction of microstructural defects can be an effective way to enhance the multifunctional properties of these alloys.

This work has been carried out with the financial support of the Spanish "Ministerio de Economía y Competitividad" (Projects number MAT2015-65165-C2-R) and of the Basque Government (Grant No. IT-1005-16). We also acknowledge ILL and SpINS for beam time

allocation: experiments 5-24-591 (<http://dx.doi.org/10.5291/ILL-DATA.5-24-591>) and CRG-2352. J. López-García acknowledges ILL for his Ph. D. contract and I. Unzueta also wants to thank the Basque Government Grant No. PRE-2014-1-214.

References

- [1] E. Sasioglu, L.M. Sandratskii, P. Bruno, *Phys. Rev. B* 70 (2004) 024427.
- [2] E. Sasioglu, L. M. Sandratskii, and P. Bruno, *Phys. Rev. B* 77 (2008) 064417.
- [3] V. D Buchelnikov, P. Entel, S. V Taskaev, V. V. Sokolovskiy, A. Hucht, M. Ogura, H. Akai, M. E. Gruner, and S.K. Nayak, *Phys. Rev. B* 78 (2008) 184427.
- [4] R. Kainuma, Y. Imano, W. Ito, Y. Sutou, H. Morito, S. Okamoto, K. Kitakami, A. Oikawa, O. Fujita, T. Kanomata, and K. Ishida, *Nature* 439 (2006) 957.
- [5] K. Koyama, K. Watanabe, T. Kanomata, R. Kainuma, K. Oikawa, and K. Ishida, *Appl. Phys. Lett.* 88 (2006) 132505.
- [6] K. Oikawa, W. Ito, Y. Imano, Y. Sutou, R. Kainuma, K. Ishida, S. Okamoto, O. Kitakami, and T. Kanomata, *Appl. Phys. Lett.* 88 (2006) 122507.
- [7] M. Acet, Ll. Mañosa, and A. Planes, in: K.H.J. Buschow (Ed), *Handbook of magnetic materials Vol.19*, Elsevier, Amsterdam, 2011, pp. 231-289.
- [8] R. Kainuma, W. Ito, R. Y. Umetsu, and V. V. Khovaylo, *Mater. Sci. Forum* 684 (2011) 139.
- [9] S. Y. Yu, Z. H. Liu, G. D. Liu, J. L. Chen, Z. X. Cao, G. H. Gu, B. Zhang, and X. X. Zhang, *Appl. Phys. Lett.* 89 (2006) 162503.
- [10] V. K. Sharma, M. K. Chattopadhyay, K. H. B. Shaeb, A. Chouhan, and S. B. Roy, *Appl. Phys. Lett.* 89 (2006) 222509.
- [11] T. Krenke, E. Duman, M. Acet, E. F. Wassermann, X. Moya, Ll. Mañosa, and A. Planes, *Nat. Mat.* 4 (2005) 450.
- [12] T. Krenke, E. Duman, M. Acet, E. F. Wassermann, X. Moya, Ll. Mañosa, A. Planes, E. Suard, and B. Ouladdiaf, *Phys. Rev. B* 75 (2007) 104414.
- [13] A. Planes, Ll. Mañosa, and M. Acet, *J. Phys.: Condens. Matter.* 21 (2009) 233201.
- [14] J. Liu, T. Gottschall, K. P. Skokov, J. K. Moore, and O. Gutfleisch, *Nature Mater.* 11 (2012) 620.

- [15] Y. Sutou, Y. Imano, N. Koeda, T. Omori, R. Kainuma, K. Ishida, and K. Oikawa, *Appl. Phys. Lett.* 85 (2004) 4358.
- [16] T. Krenke, M. Acet, E. F. Wassermann, X. Moyà, Ll. Mañosa, and A. Planes, *Phys. Rev. B* 72 (2005) 014412.
- [17] T. Krenke, M. Acet, E. F. Wassermann, X. Moyà, Ll. Mañosa, and A. Planes, *Phys. Rev. B* 73 (2006) 174413.
- [18] M. Khan, I. Dubenko, S. Stadler, and N. Ali, *J. Phys.: Condens. Matter.* 20 (2008) 235204.
- [19] V. Recarte, J. I. Pérez-Landazábal, V. Sánchez-Alarcos, and J. A. Rodríguez-Velamazán, *Acta Mater.* 60 (2012) 1937.
- [20] V. Recarte, J. I. Pérez-Landazábal, and V. Sánchez-Alarcos, *J. Alloy. Comp.* 536 (2012) S308.
- [21] V. Sánchez-Alarcos, V. Recarte, J. I. Pérez-Landazábal, E. Cesari, and J. A. Rodríguez-Velamazán, *Entropy* 16 (2014) 2756.
- [22] V. Sánchez-Alarcos, J. I. Pérez-Landazábal, V. Recarte, I. Lucia, J. Vélez, and J. A. Rodríguez-Velamazán, *Acta Mater.* 61 (2013) 4676.
- [23] A. L. Alves, E. C. Passamani, V. P. Nascimento, A. Y. Takeuchi, and C. J. Larica, *J. Phys. D: Appl. Phys.* 43 (2010) 345001.
- [24] E. C. Passamani, V. P. Nascimento, C. J. Larica, A. Y. Takeuchi, A. L. Alves, J. R. Proveti, M. C. Pereira, and J. D. Fabris, *J. Alloy. Comp.* 509 (2011) 7826.
- [25] A. Ghotbi Varzaneh, P. Kameli, V. R. Zahedi, F. Karimzadeh, and H. Salamati, *Met. Mater. Int.* 4 (2015) 758.
- [26] P. Czaja, J. Przewoznik, M. Fitta, M. Balanda, A. Chrobak, B. Kania, P. Zackiewicz, A. Wójcik, M. Szlezzynger, and W. Maziarz, *J. Magn. Magn. Mater.* 401 (2016) 223.
- [27] X. Wang, F. Sun, J. Wang, Q. Yu, Y. Wu, H. Hua, and C. Jiang, *J. Alloy. Comp.* 691 (2017) 215.
- [28] I. Unzueta, J. Lopez-García, V. Sánchez-Alarcos, V. Recarte, J. I. Pérez-Landazábal, J. A. Rodríguez-Velamazán, J. S. Garitaonandia, J. A. García, and F. Plazaola, *Appl. Phys. Lett.* 110 (2017) 181908.
- [29] Y. Murakami, K. Yanagisawa, K. Niitsu, H. S. Park, T. Matsuda, R. Kainuma, D. Shindo, and A. Tonomura, *Acta Mater.* 61 (2013) 2095.
- [30] R. Kainuma, Y. Imano, W. Ito, H. Morito, Y. Sutou, K. Oikawa, A. Fujita, K. Ishida, S. Okamoto, O. Kitakami, and T. Kanomata, *Appl. Phys. Lett.* 88 (2006) 192513.
- [31] A. K Nayak, K.G. Suresh, and A.K. Nigam, *J. Phys. D: Appl. Phys.* 42 (2009) 035009.
- [32] L. Huang, D. Y. Cong, H. L. Suo, and Y. D. Wang, *Appl. Phys. Lett.* 104 (2014)132407.
- [33] R. Y. Umetsu, A. Sheikh, W. Ito, B. Ouladdiaf, K. R. A. Ziebeck, T. Kanomata, and R. Kainuma, *Appl. Phys. Lett.* 98 (2011) 042507.

- [34] J. Rodríguez-Carvajal, *Physica B* 192 (1993) 55.
- [35] V. Sánchez-Alarcos, V. Recarte, J. I. Pérez-Landazábal, C. Gómez-Polo, and J.A. Rodríguez-Velamazán, *Acta Mater.* 60 (2012) 3168.
- [36] V. V. Khovaylo, T. Kanomata, T. Tanaka, M. Nakashima, Y. Amako, R. Kainuma, R. Y. Umetsu, H. Morito, and H. Miki, *Phys. Rev. B* 80 (2009) 144409.
- [37] S. Chikazumi, *Physics of Magnetism*, Willey, 1964.
- [38] E.J. Schlomann, *J. Appl. Phys.* 38 (1967) 5027.
- [39] H. Zhang, D. Zeng, Z. Liu, *J. Magn. Magn Mater.* 322 (2010) 2375.
- [40] G.F. Donne, J.A. Weiss, A.A. Gary, *J. Appl. Phys.* 61 (1987) 3862.
- [41] X. Moya, Ll. Mañosa, A. Planes, S. Aksoy, M. Acet, E. F. Wassermann, and T. Krenke, *Phys. Rev. B* 75 (2007) 184412.
- [42] V. Recarte, J. I. Pérez-Landazábal, V. Sánchez-Alarcos, V. Zablotskii, E. Cesari, and S. Kustov, *Acta Mater.* 60 (2012) 3168.
- [43] J. López-García, I. Unzueta, V. Sánchez-Alarcos, V. Recarte, J. I. Pérez-Landazábal, J. A. Rodríguez-Velamazán, J. A. García, and F. Plazaola, *Intermetallics* 94 (2018) 133.
- [44] M. Forsblom, N. Sandberg, and G. Grimvall, *Phil. Mag.* 84 (2004) 521.
- [45] P. C. Shuck, J. Marian, J. B. Adams, and B. Sadigh, *Phil. Mag.* 89 (2009) 2861.
- [46] V. R. Manga, S. L. Shang, W. Y. Wang, Y. Wang, J. Liang, V. H. Crespi, and Z. K. Liu, *Acta Mater.* 82 (2015) 287.

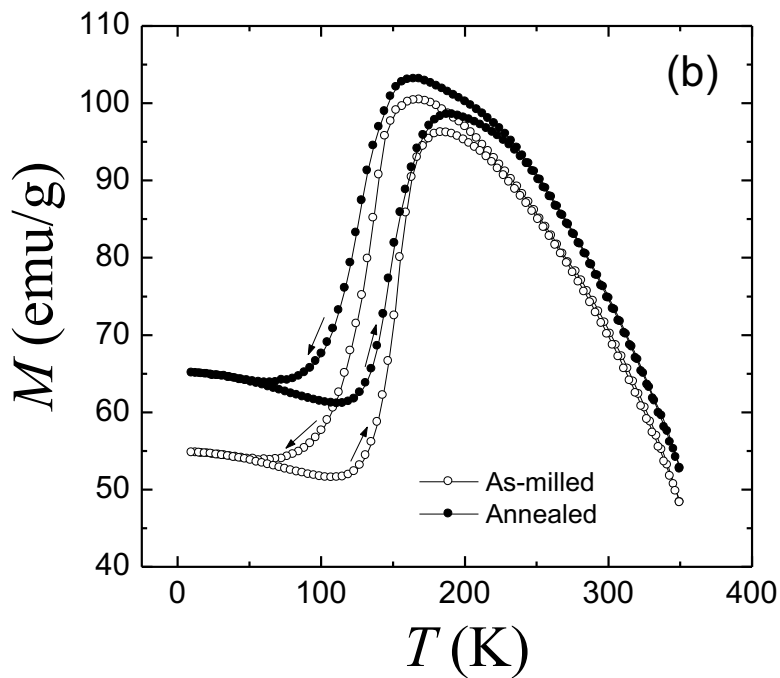
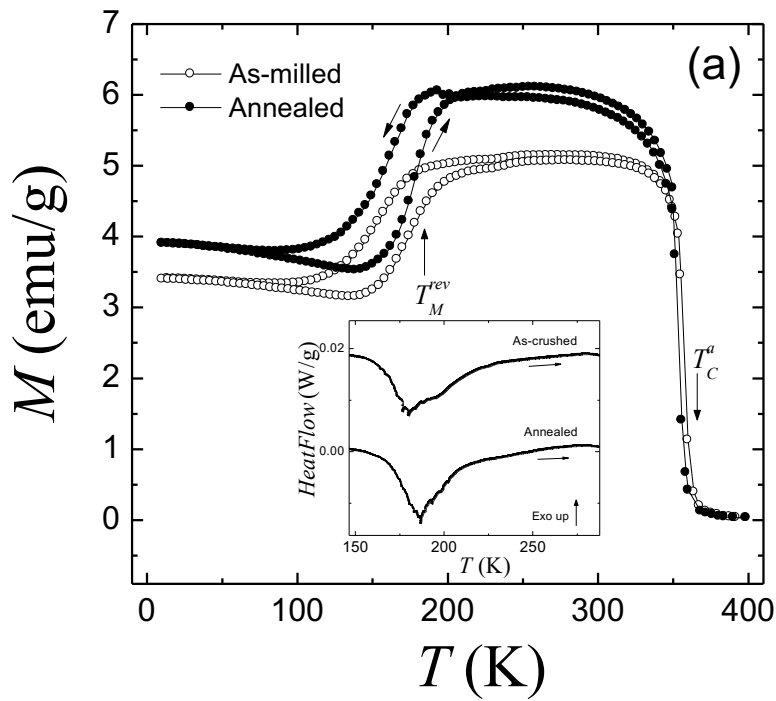


Fig.1

Sánchez-Alarcos et al.

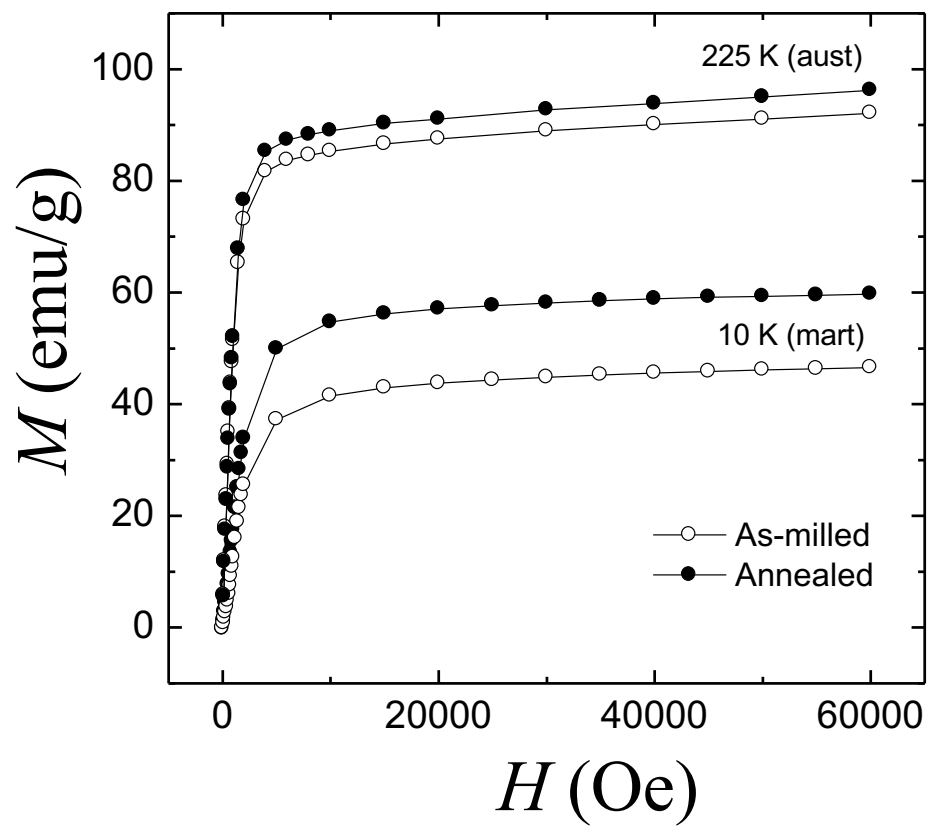


Fig.2

Sánchez-Alarcos et al.

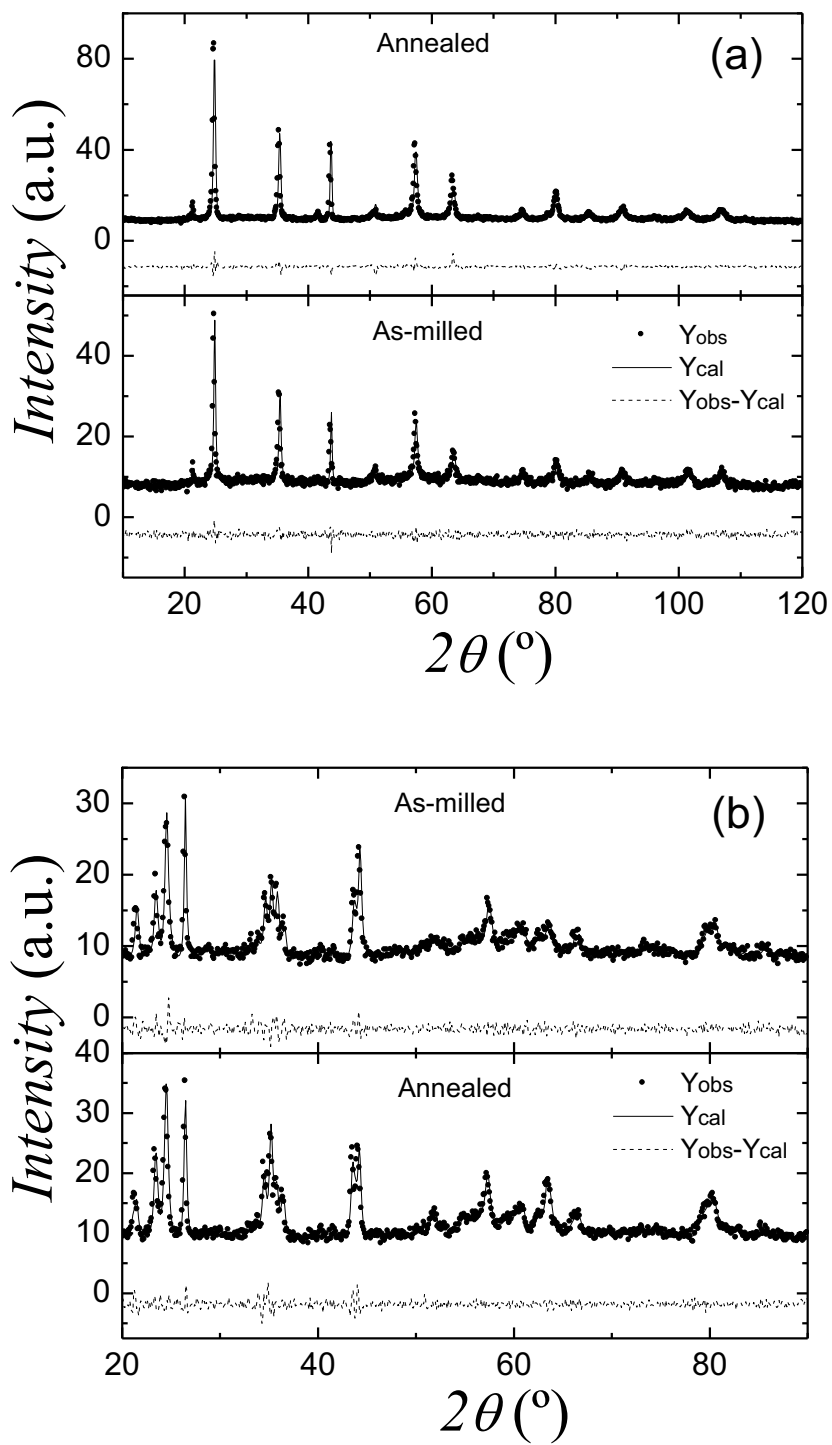


Fig.3

Sánchez-Alarcos et al.

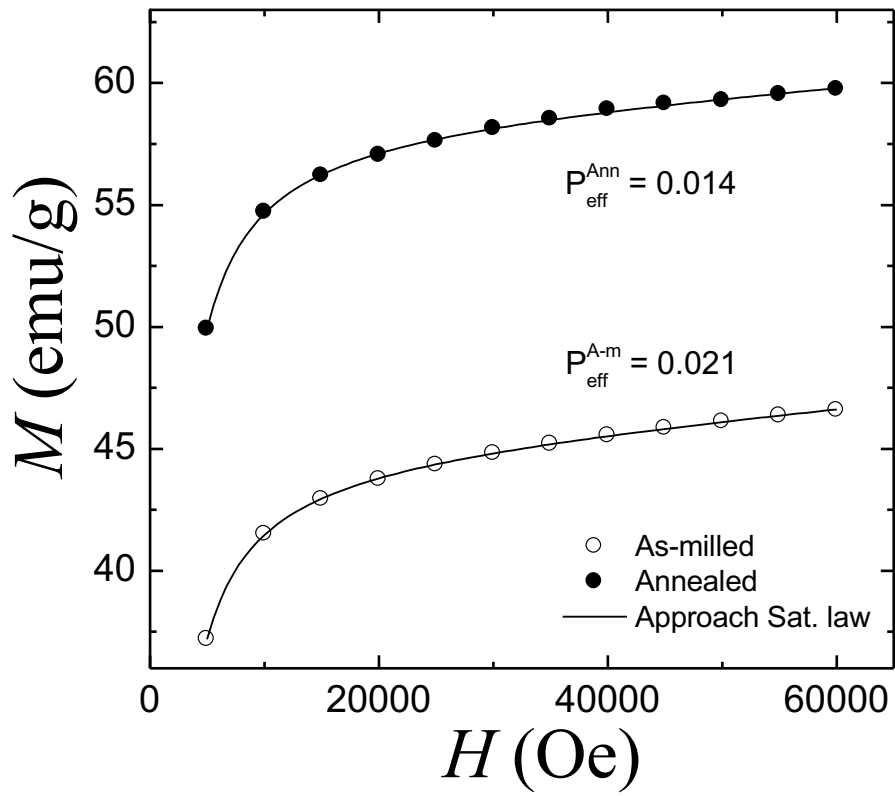


Fig.4

Sánchez-Alarcos et al.

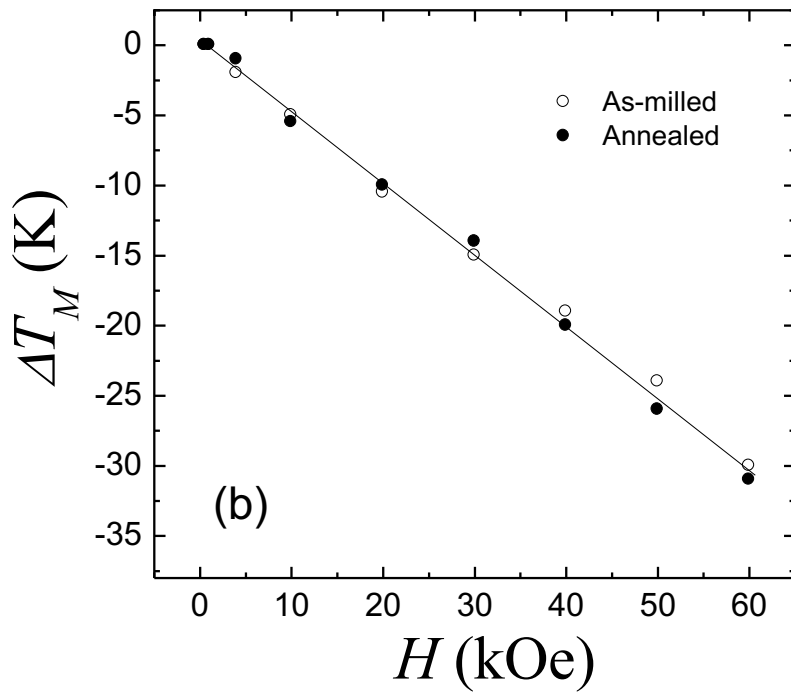
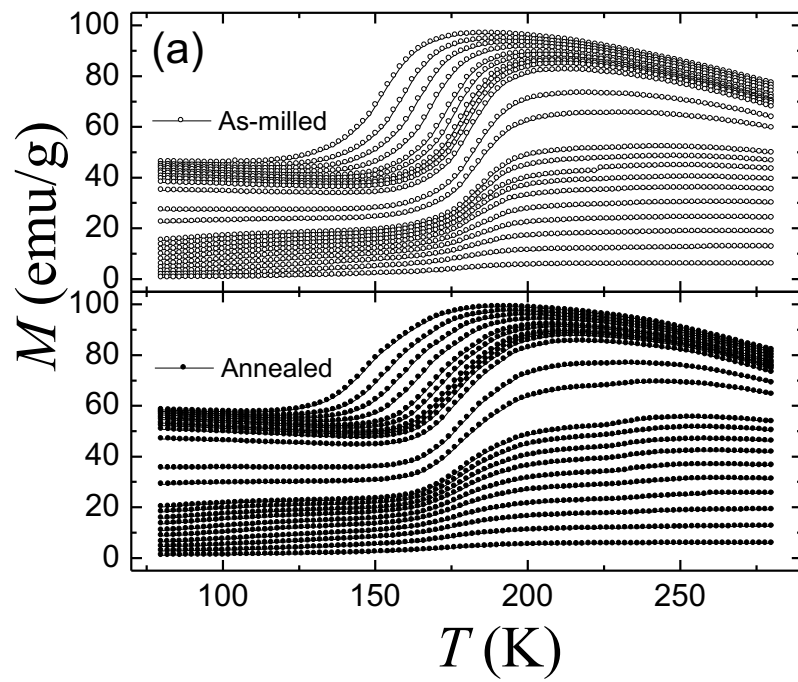


Fig.5

Sánchez-Alarcos et al.

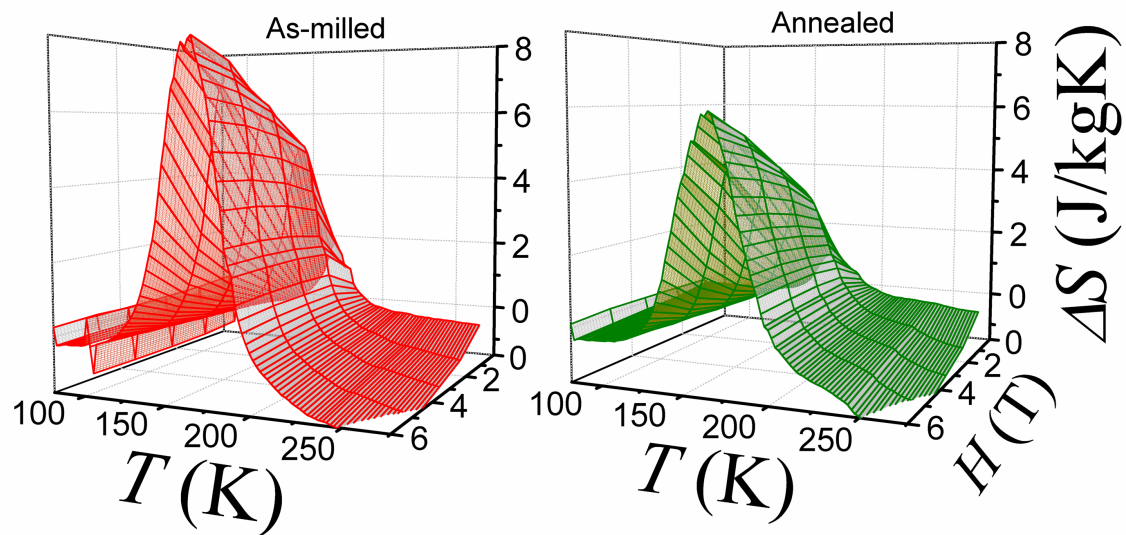


Fig.6

Sánchez-Alarcos et al.

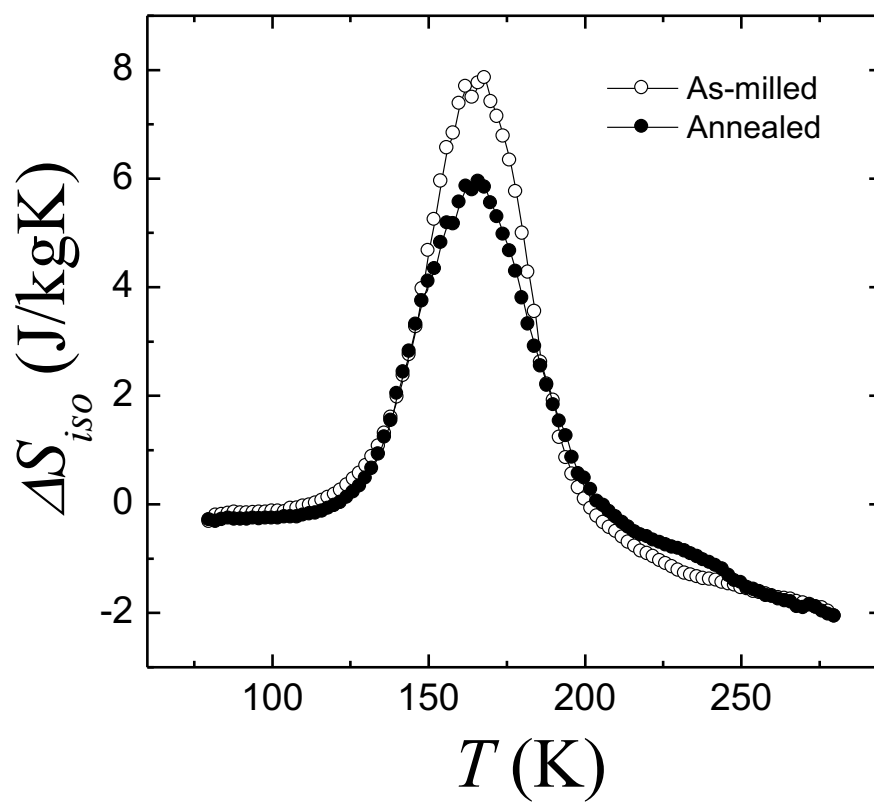


Fig.7

Sánchez-Alarcos et al.

<i>Sample</i>	T_M^{rev} (100 Oe) (K)	T_M^{rev} (60 kOe) (K)	T_C^a (K)	ΔM (emu/g)	ΔS (J/kgK)
As-milled	187	159	362	52	9.8
Annealed	188	159	360	40	8.1

Table 1

Sánchez-Alarcos et al.

State	Cubic $Fm\bar{3}m$			Monoclinic $P2/m$	
	Site	Atom	μ (μ_B)	Site	μ (μ_B)
As-milled	4a	0.94Mn+0.06Sn	3.11(2)	1a, 1h, 2n, 2m	2.47 (10)
	4b	0.47Mn+0.53Sn	1.14(2)	1b, 1g, 2m', 2n'	-0.91(10)
	8c	0.88Ni+0.12Co	0.296*	2j, 2k, 4o, 4o'	0.296*
Annealed	4a	0.97Mn+0.03Sn	3.11(2)	1a, 1h, 2n, 2m	2.50(21)
	4b	0.49Mn+0.51Sn	1.19(2)	1b, 1g, 2m', 2n'	-0.56(41)
	8c	0.90Ni+0.10Co	0.28*	2j, 2k, 4o, 4o'	0.28*

Atomic positions: 2n: x = 0.397(1), z = 0.201 (1); 2m: x = 0.032(1), z = 0.326 (1); 2m': x = -0.034(4), z = 0.201 (1); 2n': x = 0.453(5), z = 0.326 (1); 2j: y = 0.245(13); 2k: y = 0.221(7); 4o: z = 0.201 (1); 4o': z = 0.326 (1)

Table 2

Sánchez-Alarcos et al.